Multi-scale (time and mass) dynamics of space objects
Proceedings IAU Symposium No. 364, 2022
A. Celletti, C. Galeş, C. Beaugé, A. Lemaitre, eds.
doi:10.1017/S1743921322000461

A numerical criterion evaluating the robustness of planetary architectures; applications to the υ Andromedæ system

Ugo Locatelli[1], Chiara Caracciolo[2], Marco Sansottera[2] and Mara Volpi[1]

[1]Dipartimento di Matematica dell'Università degli Studi di Roma "Tor Vergata", via della ricerca scientifica 1, 00133 Roma, Italy
emails: locatell@mat.uniroma2.it, volpi@mat.uniroma2.it

[2]Dipartimento di Matematica dell'Università degli Studi di Milano, via Saldini 50, 20133 Milano, Italy
emails: chiara.caracciolo@unimi.it, marco.sansottera@unimi.it

Abstract. We revisit the problem of the existence of KAM tori in extrasolar planetary systems. Specifically, we consider the υ Andromedæ system, by modelling it with a three-body problem. This preliminary study allows us to introduce a natural way to evaluate the robustness of the planetary orbits, which can be very easily implemented in numerical explorations. We apply our criterion to the problem of the choice of a suitable orbital configuration which exhibits strong stability properties and is compatible with the observational data that are available for the υ Andromedæ system itself.

Keywords. Planetary Systems, Celestial Mechanics.

1. Introduction

From the very beginning of their history, physical sciences have been an inexhaustible source of problems and inspiration for mathematics. In particular, the orbital characteristics of more and more extrasolar systems are raising very challenging questions which concern the modern theory of stability for planetary Hamiltonian systems.

Since the announcement of the discovery of the first one (Mayor & Queloz 1995), thousands of exoplanets have been detected. Systems hosting more than one planet show a rather surprising variety of configurations which can be remarkably different with respect to that of the Solar System, which presents planetary orbits that are well separated, quasi-circular and nearly coplanar. The situation is made even more complex by the fact that none of the detection methods nowadays available to discover extrasolar planets is able to measure all their orbital elements. In this regard, the Radial Velocity (hereafter, RV) method is the most effective observation technique, because it provides values for the semi-major axis a, the eccentricity e, and the argument of the pericentre ω of an exoplanet (see, e.g., Perryman 2018). Moreover, the RV method is able to evaluate the so-called minimal mass $m\sin(\iota)$, where m and ι are the mass and the inclination† of the observed exoplanet, respectively. Indeed, this is as a very serious limitation of the currently available detection techniques, since they are often unable to completely determine

† More precisely, ι refers to the inclination of the Keplerian ellipse with respect to the plane orthogonal to the line of sight (i.e., the direction pointing to the object one is observing), which is usually said to be "tangent to the celestial sphere".

such an important parameter like the mass of an exoplanet (which is crucial to draw conclusions about, e.g., its habitability). In particular, the three-dimensional architecture of a multi-planetary system eludes the observational measures, when they are made using the RV method. However, this can be determined by crossing the results provided by multiple detection techniques, when different methods can be applied to the same system. Since the transit photometry is the most prolific technique in the discovering of exoplanets, its joined use with the RV method is expected to be very promising for what concerns their orbital characterisation. For instance, the combination of the transit and the RV method allowed to measure the inclination of three exoplanets orbiting around the L 98-59 star and so to determine rather narrow ranges for the values of their masses (Cloutier et al. 2019). Although the data obtained through astrometry are less precise with respect to the aforementioned detection techniques, they can be joined with the measures provided by the RV method to evaluate both the inclination ι and the longitude of the node Ω for some massive-enough exoplanets (e.g., in the case of HD 128311 *c*, see McArthur et al. 2014). Moreover, combining astrometry and RV methods it was possible to determine ranges of values for all the orbital elements except the mean anomalies M for the two exoplanets that are expected to be the most massive ones among those orbiting the υ Andromedæ A star† (McArthur et al. 2010). On one hand, this allowed to describe rather carefully the 3D structure of the main part of this extrasolar system, with an instantaneous value of the mutual inclination of $29.9^\circ \pm 1^\circ$; on the other hand, the uncertainty on the knowledge of a few orbital elements is so large that the estimated error on the mass of one of the exoplanets is quite relevant (i.e., $\simeq 30\%$), which is also due to the fact that its orbital plane is very inclined with respect to the line of sight.

According to the approach designed by Morbidelli & Giorgilli (1995), the stability of quasi-integrable systems can be efficiently analysed by combining the KAM theorem with the Nekhoroshev's one. In fact, their joint application can ensure the effective stability (that is valid for interval of times larger than the estimated age of the universe) for Hamiltonian systems of physical interest. This strategy has been successfully applied to a pair of non-trivial planetary models describing the dynamics of the two or three innermost Jovian planets of our Solar System; in both those cases, upper bounds on the diffusion speed have been provided by suitable estimates on the remainder of the Birkhoff normal form which is preliminarily constructed in the neighbourhood of an invariant torus (Giorgilli et al. 2009 & 2017). The so-called Arnold diffusion is a phenomenon which cannot take place in Hamiltonian systems having two degrees of freedom (hereafter, d.o.f.), because 2D invariant tori act as topological barriers separating the orbits. Nevertheless, reverse KAM theory can be applied in a way that is far from being trivial for what concerns the secular dynamics of extrasolar systems including three bodies (which can be described by a Hamiltonian model with 2 d.o.f.). In fact, in Volpi et al. (2018) the explicit construction of invariant KAM tori is used to infer information on the possible ranges of values of the mutual inclinations between the orbital planes of the two exoplanets hosted in the three following systems: HD 141399, HD 143761 and HD 40307. However, such an approach suffers serious limitations, mainly due to the fact that is based on an algorithm which was designed to construct suitable normal forms for the secular dynamics of our Solar System (Locatelli & Giorgilli 2000). Firstly, this computational procedure is apparently unable to deal with the case of eccentricities larger than 0.1, which is quite frequent

† Indeed, υ Andromedæ is a binary star. Since the companion is a red dwarf that is quite far (about 750 AU) from the primary star, the former is expected to not appreciably affect the planetary system orbiting the latter one. For the sake of simplicity, with the name of υ Andromedæ hereafter we will refer to both its primary star (which is, more precisely, υ Andromedæ A) and the extrasolar system hosting the exoplanets that have been discovered around it.

https://doi.org/10.1017/S1743921322000461 Published online by Cambridge University Press

for exoplanets discovered by the RV detection method. Moreover, although the algorithm constructing the normal forms can work with bunches of initial conditions at the same time (if the implementation is made by using interval arithmetics, see Volpi et al. 2018), this kind of procedures can be rather demanding from a computational point of view, if they are not tailored carefully to the model under consideration. Therefore, the possibility to apply extensively such an approach to the study of many extrasolar systems looks rather doubtful. The so-called criterion of the Angular Momentum Deficit (hereafter AMD, see Laskar & Petit 2017, and Petit et al. 2017 for its reformulation adapted to planetary systems in mean motion resonance) gives an elegant answer to the need of a "coarse-graining" method for quickly studying the stability of many extrasolar planetary systems. However, also the AMD criterion does not cover all the extrasolar planetary systems that are known up to now, in the sense that is unable to ensure the stability for some of them. In particular, the AMD criterion can become inapplicable to systems where the orbital plane of (at least) one exoplanet is highly inclined with respect to the line of sight; for instance, this is exactly what occurs in the case of υ Andromedæ, which is very challenging. On the one hand, the 2D three-body model which includes the star and its two exoplanets with the largest minimal masses looks stable according to the AMD criterion, when the line of sight lies in their common orbital plane (Fig. 7 of Laskar & Petit 2017). On the other hand, when also the inclinations and the longitudes of the nodes are taken into account, then there is a remarkable fraction of the possible initial conditions that generates motions which are evidently unstable (McArthur et al. 2010; Deitrick et al. 2015). This is mainly due to the fact that the actual value of the mass of υ And c should be larger than 5 times the minimal one, while the increasing factor affecting the value of υ And d's mass is about 2.5 . Therefore, the perturbation of the Keplerian orbits (that is mainly due to the mutual gravitation) due to the updated values of the exoplanetary masses is one order of magnitude larger than the perturbation in the two-dimensional models of the υ Andromedæ system considering the data derived by the first observational measures provided by the RV detection method.

In Caracciolo et al. 2022, we have studied the secular dynamics of the υ Andromedæ system by adopting the so called averaged model at order two in the masses. In that framework we have shown how to construct an invariant (KAM) manifold which is a very accurate approximation of the orbit originating from initial conditions that are within the range of the observed values. Moreover, we have also shown rigorously the existence of such a KAM torus, by adopting a suitable technique based on a computer-assisted proof. Let us recall that this ensures that there is a small region around those initial conditions (and so, consistent with the observational data) for which the secular dynamics is effectively stable (see again the aforementioned paper by Morbidelli & Giorgilli 1995). Indeed, we have carefully selected those initial conditions by using a numerical criterion to evaluate the *robustness* of the corresponding orbit. The present work is devoted to the description of such a criterion. As it will be discussed in the next sections, the concept of robustness actually refers to the eventually existing torus which covers the orbit. The key remark which allows us to introduce such a criterion can be shortly summarised as follows: for what concerns the secular dynamics of the υ Andromedæ system, a KAM torus is as more persistent to the perturbing terms as it is closer to a periodic orbit which corresponds to the anti-alignment of the pericentre arguments of υ And c and υ And d. Thus, it is natural to apply our robustness criterion in situations where the exoplanets are in a librational regime with respect to the difference of their pericentre arguments. Let us recall that υ And c and υ And d were conjectured to be in such an apsidal locking state just a few years after their discovery (Chiang et al. 2001, see also Michtchenko & Malhotra 2004 for an explanation of such a dynamical mechanism within the framework of a secular model). Although our robustness criterion

https://doi.org/10.1017/S1743921322000461 Published online by Cambridge University Press

Table 1. Orbital elements and minimal masses of the exoplanets υ And c and υ And d. All the data appearing in the following first three columns are reported from Table 13 of McArthur et al. (2010). In the rightmost column we have included also the relative errors for each quantity. In all our numerical integrations the stellar mass of υ Andromedæ is assumed to be $m_0 = 1.31\ M_\odot$. As usual, $M_\odot$ and M_J denote the solar mass and the Jupiter one, respectively.

	υ **And** c	υ **And** d	**rel. err.**
$a(0)$ [AU]	0.829 ± 0.043	2.53 ± 0.014	$\simeq 5\,\%$
$e(0)$	0.245 ± 0.006	0.316 ± 0.006	$\simeq 5\,\%$
$\iota(0)$ [°]	7.868 ± 1.003	23.758 ± 1.316	1.4/180
$\omega(0)$ [°]	247.66 ± 1.76	252.99 ± 1.31	1.8/360
$\Omega(0)$ [°]	236.85 ± 7.53	4.07 ± 3.31	7.6/360
$m \sin(\iota(0))$ $[M_J]$	1.96 ± 0.05	4.33 ± 0.11	$\lesssim 3\,\%$

simply applies in combination with numerical integrations (any averaging procedure is not strictly necessary), it is somehow related with the dynamical phenomenon we have described by adopting the language of the normal forms and the refined computational procedure which is fully detailed in Caracciolo et al. 2022. Therefore, our robustness numerical indicator does not aim to be as general as the AMD stability criterion, at least in its first formulation we are going to introduce; eventual extensions to contexts different with respect to the librations in an apsidal locking regime (or in the anti-apsidal one) could need some nontrivial adaptations.

2. The orbital dynamics of the exoplanets in the υ Andromedæ system: a short overview

The discovery of three exoplanets orbiting around υ Andromedæ was made at the end of the last century, by applying the RV detection method (Butler et al. 1999). Moreover, McArthur et al. (2010) remarked that a long-period trend in the analysis of the signals is an indication of the presence of a fourth planet (named υ And e). The long-term stability of a planetary system which includes υ And b, υ And c and υ And d has been studied in Deitrick et al. 2015, by performing many numerical integrations; let us also recall that several of them have shown unstable motions. In the present work, we are going to further restrict the model by limiting us to consider the two exoplanets that are expected to be the largest ones. There are good reasons to assume that the influence exerted by υ And b and υ And e is negligible: the latter is known quite poorly (and the RV method is rather sensitive to more massive bodies), while the former is very tightly close to the star and its minimal mass is one order of magnitude smaller than the ones of υ And b and υ And c†.

The initial values of the orbital elements (except the mean anomalies, that are unknown) for the pair of exoplanets υ And c, υ And d and their minimal masses are reported in Table 1. Hereafter, in our three-body model of the υ Andromedæ extrasolar system the indexes 1, 2 will be used to refer to the inner planet and the outer one, respectively, while m_0 will denote the stellar mass. Looking at Table 1, one can appreciate that all the reported data are given with a relative uncertainty that is not larger than a few percentage units. Due to the occurrence of the increasing factor $1/\sin(\iota_j(0))$ (with $j = 1, 2$), this is no more true for the exoplanetary masses. A straightforward evaluation starting from the data reported in Table 1 gives $m_1 = 14.6 \pm 2.2$ and $m_2 = 10.8 \pm 0.9$. Therefore, the relative uncertainty of at least one parameter (which plays a crucial role

† The ratio between the semi-major axes of two consecutive planets is $\simeq 14$ in the case of the pair υ And c – υ And b, while it is a bit more than 3 in the case of υ And d – υ And c. In the case of υ And b the value of the quantity $m \sin(\iota(0))$ is known to be $0.0594 \pm 0.0003\ M_J$ (see Table 13 of McArthur et al. (2010), whose data concerning υ And c and υ And d are reported in our Table 1 above). Let us also recall that the initial inclination $\iota(0)$ of υ And b is unknown and, thus, the minimal value is the only information available about its mass.

https://doi.org/10.1017/S1743921322000461 Published online by Cambridge University Press

Table 2. List of the values of the parameters that are kept fixed in all our numerical explorations. In the first two rows, the initial conditions concerning with semi-major axes and eccentricities of the exoplanets υ And c and υ And d are reported. In the last row, their values of the minimal masses are given.

	υ **And** c	υ **And** d
$a(0)$ [AU]	0.829	2.53
$e(0)$	0.239	0.310
$m\sin(\iota(0))$ $[M_J]$	1.91	4.22

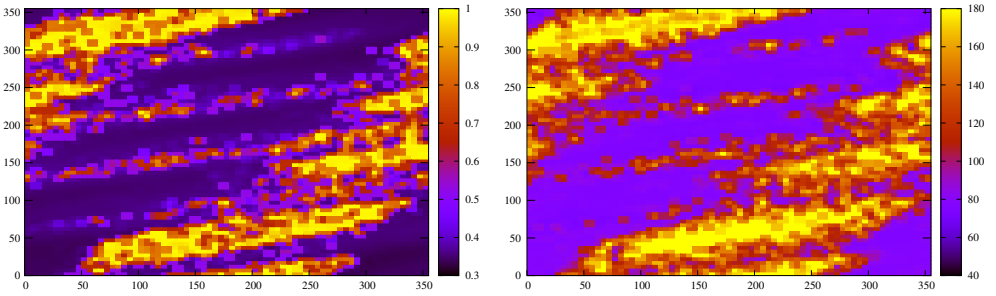

Figure 1. On the left, a colour-grid plot of the maximal value reached by the eccentricity e_2 of υ And d. On the right, the same for the maximal value of the difference between the pericentres, i.e., $\max_t\ |\omega_1(t)-\omega_2(t)|$. In both panels, the plots are made as a function of the initial values of the mean anomalies $M_1(0)$ and $M_2(0)$. See the text for more details about the choice of the initial conditions.

in the discussion about the stability of this extrasolar planetary system) can reach† 15 % of the corresponding mid value; this is the case of the mass of υ And c.

We emphasise that an extensive study of the possible motions with an homogeneous and accurate covering of all the possible initial conditions and parameters gets immediately far too complex from a computational point of view, because it would require to deal with a fourteen-dimensional grid. For the sake of simplicity, we started to reduce the complexity by fixing some of the parameters that are determined rather precisely by the observational measures made by using the RV method; in detail, they are two pairs of orbital elements, i.e., the initial values of semi-major axes and eccentricities, and the minimal masses. The latter two pairs have been fixed so to be equal to the lowest possible values of the corresponding ranges given in Table 1. This choice has been made in order to increase the fraction of the orbital motions that are apparently stable. All the values of the parameters that have been so fixed by us are reported in Table 2.

We start our numerical explorations by investigating the dependence on the pair of the orbital elements that are unknown, namely the mean anomalies M_1 and M_2 ‡. For this purpose, we decide to consider sets of initial conditions such that $\iota_j(0)$, $\omega_j(0)$ and $\Omega_j(0)$ are set to be equal to the corresponding mid values reported in Table 1, $\forall\ j=1,2$. Moreover, the initial conditions are complemented with the data reported in Table 2, while the initial values of the mean anomalies are taken from a regular 2D grid covering all the set $[0°,360°]\times[0°,360°]$ with a grid-step of 5°. Hereafter, the mass of each exoplanet is always determined by multiplying its minimal value (appearing in Table 2) by the

† Taking into account all the uncertainties due to the observational measures, the errors ranges are even wider. Indeed, in Table 13 of McArthur et al. (2010) the following values for the exoplanetary masses are given: $m_1=13.98^{+2.3}_{-5.3}$ and $m_2=10.25^{+0.7}_{-3.3}$.

‡ The observational data reported in both online catalogues and published papers determine values for the orbital period and the epoch of periastron. From these two values it is possible to infer the values of the mean anomalies, but they are never explicitly determined. In this respect, we then consider them as *unknown*.

https://doi.org/10.1017/S1743921322000461 Published online by Cambridge University Press

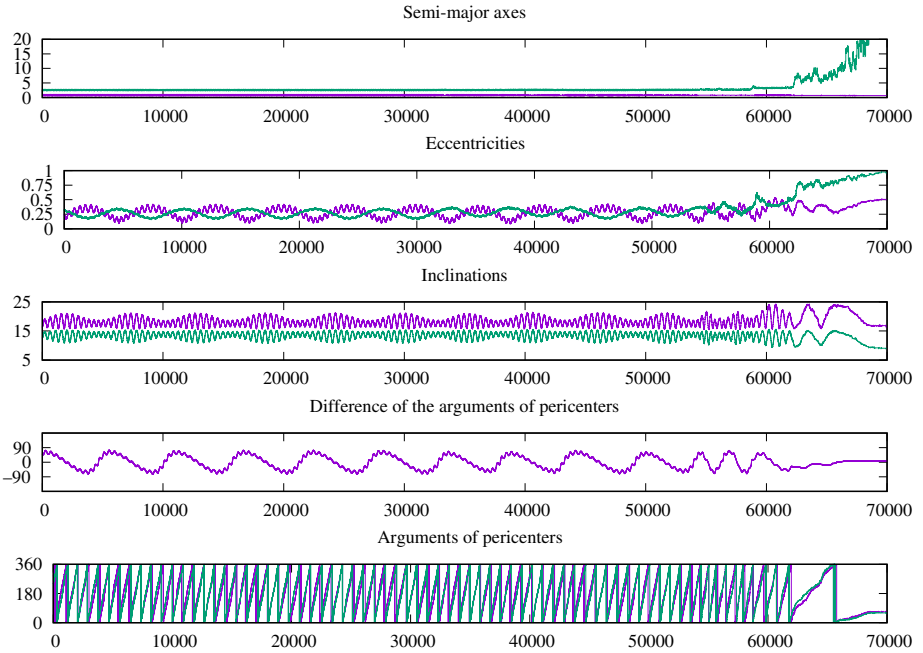

Figure 2. Orbital evolution of the exoplanets υ And c and υ And d in the case of one single set of initial conditions among those that have been considered also in Fig. 1 with the particular choice $M_1(0) = 0^\circ$ and $M_2(0) = 120^\circ$ for what concerns the initial values of the mean anomalies. From top to bottom, the five graphs include the plots of the evolution for the following quantities: semi-major axes a_1 and a_2 , eccentricities e_1 and e_2 , inclinations ι_1 and ι_2 , difference of the arguments of the pericentres $\omega_2 - \omega_1$, arguments of the pericentres ω_1 and ω_2 . The plots in green refer to the orbital motion of υ And d. The inclinations are evaluated with respect to the direction of the total angular momentum. In all the abscissas, the year is assumed as unit of measure of time.

corresponding increasing factor $1/\sin(\iota(0))$. Starting from each of the initial conditions defined just above, we have numerically integrated the Hamilton equations describing our three-body planetary model, by using the symplectic method $\mathcal{SBAB}_{\mathcal{C}3}$ as it is defined in Laskar & Robutel (2001) for a timespan of 10^5 yr, with an integration step of 0.02 yr. The main results so obtained are summarised in Fig. 1, which highlights that the choice of the initial values of the mean anomalies affects the orbital dynamics in a very remarkable way. In fact, the regions that appear with lighter colours in the left panel correspond to motions that can experience close encounters. Let us recall that the threshold value of the eccentricity of the outer planet on top of which collisions with the inner planet are possible can be roughly evaluated as $1 - (a_1(0)/a_2(0)) \simeq 0.67$. On the other hand, about 50 % of the colour-grid plot in the left panel is in dark; this means that the maximum value of the eccentricity of the outer planet looks to be safely below that threshold allowing close encounters with the inner one. The strong similarity between the two panels of Fig. 1 clearly suggests that stable configurations are possible when the difference of the pericentre arguments is in a librational regime, i.e., the orbital motions are such that the maximum of the half-width of the oscillations concerning with $\omega_1(t) - \omega_2(t)$ is less than 180°. Let us emphasise that this kind of phenomena has already been observed in the last few years. In fact, the relevance of the impact due to the mean anomalies on the orbital dynamics of extrasolar systems that are close or in mean motion resonance has been shown, e.g., in Libert & Sansottera (2013) and Sansottera & Libert (2019).

https://doi.org/10.1017/S1743921322000461 Published online by Cambridge University Press

In order to make clear the ideas, it can be convenient to have a close look at the dynamical evolution of most of the orbital elements, for a motion starting form one single set of initial conditions, that is selected among those considered in Fig. 1. In particular, the orbital evolution described by the plots included in Fig. 2 refers to $M_1(0) = 0^\circ$ and $M_2(0) = 120^\circ$; let us recall that the other values of the initial conditions are taken from the mid values of Table 1 (for what concerns $\iota(0)$, $\omega(0)$ and $\Omega(0)$ only) and from Table 2 (for the remaining data). Looking at the plots of the orbital elements one can appreciate that the orbit is unstable; for any of those plots, the lack of quasi-periodicity is particularly evident after 50000 yr. From the behaviour of the semi-major axes and the eccentricities, it is obvious that the outer planet is ejected from the system at the end of the numerical simulation. Let us also stress that our standard implementation of the symplectic method $\mathcal{SBAB}_{\mathcal{C}3}$ usually crashes for all the motions starting from initial conditions which correspond to regions of lighter colour in the plot of the left panel in Fig. 1.

Hereafter, we will refer to the three-body planetary problem that has been described in the present section as the *complete* model, in order to distinguish it with respect to the *secular* one. The latter is an Hamiltonian system which is defined by a suitable procedure of averaging that will be briefly discussed in the next section.

3. The construction of invariant tori in the secular dynamics of the υ Andromedæ system as a source of inspiration

The present section is devoted to recall some of the ideas we recently used in order to successfully construct KAM tori, that are invariant for the secular dynamics of the υ Andromedæ planetary system and are also in librational regime with respect to the difference of the pericentre arguments (Caracciolo et al. 2022). Our aim is to explain in a rather natural way the reasons to introduce our numerical criterion evaluating the robustness of planetary configurations, that will be properly defined in the next section.

In the case of the secular dynamics of the υ Andromedæ planetary system, the preliminary construction of the normal form for a particular elliptic torus is essential to be performed before the one constructing the final KAM torus. These two constructive procedures can be described in an unified way, as we explained in Locatelli et al. (2022). We defer the reader to those pedagogical notes for all the details about this kind of (so-called) semi-analytic algorithms, that can be summarised as follows for our goals.

The proof scheme of the KAM theorem can be formulated in terms of a constructive algorithm whose convergence is ensured if some suitable hypotheses are satisfied. This procedure starts by considering an analytic Hamiltonian function $H^{(0)} : \mathcal{A} \times \mathbb{T}^n \mapsto \mathbb{R}$ (being $\mathcal{A} \subseteq \mathbb{R}^n$ an open set) of the form $H^{(0)}(\boldsymbol{p}, \boldsymbol{q}) = \boldsymbol{\nu} \cdot \boldsymbol{p} + h^{(0)}(\boldsymbol{p}, \boldsymbol{q}) + \varepsilon f^{(0)}(\boldsymbol{p}, \boldsymbol{q})$, where n denotes the number of degrees of freedom, $\boldsymbol{\nu} \in \mathbb{R}^n$ is an angular velocity vector and $h^{(0)}$ is at least quadratic with respect to the actions $\boldsymbol{p}$, i.e., $h^{(0)}(\boldsymbol{p}) = \mathcal{O}(\|\boldsymbol{p}\|^2)$ for $\boldsymbol{p} \to \boldsymbol{0}$. The term $\varepsilon f^{(0)}(\boldsymbol{p}, \boldsymbol{q})$ appearing in $H^{(0)}$ is usually called the perturbing term and it is made smaller and smaller by the normalisation procedure, which is defined by an infinite sequence of canonical transformations. This entails that we have to introduce a sequence of Hamiltonians $H^{(r)}$ that are iteratively defined so that

$$H^{(r)} = \exp\left(\mathcal{L}_{\chi_2^{(r)}}\right) \exp\left(\mathcal{L}_{\chi_1^{(r)}}\right) H^{(r-1)} \qquad \forall\ r \geq 1\ , \tag{3.1}$$

where the generating functions $\chi_1^{(r)}$ and $\chi_2^{(r)}$ are determined in such a way to remove the part of the perturbation term that is both $\mathcal{O}(\varepsilon^r)$ and not dependent on $\boldsymbol{p}$ or linear in $\boldsymbol{p}$, respectively. We then say that formula (3.1) defines the r-th normalization step. We stress that the Lie series operators $\exp\left(\mathcal{L}_{\chi_2^{(r)}}\right)$ and $\exp\left(\mathcal{L}_{\chi_1^{(r)}}\right)$ define canonical transformations when they are applied to the whole set of variables $(\boldsymbol{p}, \boldsymbol{q})$. This is due to the fact that

https://doi.org/10.1017/S1743921322000461 Published online by Cambridge University Press

they are given in terms of the Lie derivatives $\mathcal{L}_{\chi_2^{(r)}}\ \mathcal{L}_{\chi_1^{(r)}}$ (which in turn are expressed as Poisson brackets, i.e., $\mathcal{L}_g f = \{f, g\}$ for any pair of dynamical functions f and g that are defined on the phase space). The statement of the KAM theorem (see Kolmogorov 1954, Arnold 1963 and Moser 1962) can be shortly formulated as follows:

if $\boldsymbol{\nu}$ is non-resonant enough, $h^{(0)}$ is non-degenerate with respect to the actions $\boldsymbol{p}$ and the parameter ε is small enough, then there is a canonical transformation $(\boldsymbol{p}, \boldsymbol{q}) = \Psi(\boldsymbol{P}, \boldsymbol{Q})$, leading $H^{(0)}$ in the so called Kolmogorov normal form

$$\mathcal{K}(\boldsymbol{P}, \boldsymbol{Q}) = \nu \cdot \boldsymbol{P} + \mathcal{O}(\|\boldsymbol{P}\|^2)\ , \tag{3.2}$$

being $\mathcal{K} = H \circ \Psi$.

Indeed, the final canonical transformation Ψ is obtained by composing all the canonical transformations induced by $\exp\left(\mathcal{L}_{\chi_1^{(1)}}\right)$, $\exp\left(\mathcal{L}_{\chi_2^{(1)}}\right)$, ... $\exp\left(\mathcal{L}_{\chi_1^{(r)}}\right)$, $\exp\left(\mathcal{L}_{\chi_2^{(r)}}\right)$ ... Moreover, one can easily verify that the quasi-periodic motion law $t \mapsto (\boldsymbol{P}(t) = \boldsymbol{0}\ ,\ \boldsymbol{Q}(t) = \boldsymbol{Q}_0 + \boldsymbol{\nu} t)$ is the unique solution for the Hamilton equations related to the Kolmogorov normal form (3.2) with initial conditions $(\boldsymbol{P}(0)\ ,\ \boldsymbol{Q}(0)) = (\boldsymbol{0}\ ,\ \boldsymbol{Q}_0)$. Since the canonical transformations have the property of preserving solutions, then the n-dimensional KAM torus $\left\{(\boldsymbol{p}, \boldsymbol{q}) = \Psi(\boldsymbol{0}, \boldsymbol{Q})\ ,\ \forall\, \boldsymbol{Q} \in \mathbb{T}^n\right\}$ is invariant with respect the flow induced by the initial Hamiltonian $H^{(0)}$.

3.1. *Preliminaries*

As it has been first explained in Locatelli & Giorgilli (2000), the so-called secular model at order two in the masses can be properly introduced by performing a first step of normalization, which aims at removing the perturbation terms depending on the fast revolution angles. In order to set the ideas let us recall that a three-body Hamiltonian problem has nine degrees of freedom. Three of them can be easily separated because they describe the uniform motion of the centre of mass in an inertial frame. The nontrivial part of the dynamics is represented in astrocentric canonical coordinates and its degrees of freedom can be further reduced by two using the conservation of the total angular momentum $\boldsymbol{C}$. As it is shown in section 6 of Laskar (1989), this allows us to write the Hamiltonian as a function of four pairs of Poincaré canonical variables, that are

$$\begin{aligned} \Lambda_j &= \frac{m_0 m_j \sqrt{G(m_0 + m_j) a_j}}{m_0 + m_j}\ , & \xi_j &= \sqrt{2\Lambda_j}\sqrt{1 - \sqrt{1 - e_j^2}}\cos(\omega_j)\ , \\ \lambda_j &= M_j + \omega_j\ , & \eta_j &= -\sqrt{2\Lambda_j}\sqrt{1 - \sqrt{1 - e_j^2}}\sin(\omega_j)\ , \end{aligned} \qquad \forall\, j = 1, 2\ . \tag{3.3}$$

We also recall that the reduction of the total angular momentum makes implicit the dependence on the orbital elements that are missing in formula (3.3). They are the inclinations and the longitudes of the nodes, which are conveniently expressed with respect to the so-called Laplace invariant plane, that is orthogonal to the total angular momentum $\boldsymbol{C}$. However, also the instantaneous values of these two pairs of orbital elements can be recovered by the knowledge of all the others and the euclidean norm of $\boldsymbol{C}$. The actions Λ_1 and Λ_2 (that are conjugate with respect to the mean anomalies λ_1 and λ_2 , respectively) are usually expanded around a pair of reference values, namely Λ_1^* and Λ_2^*. These values are obtained by replacing the semi-major axes appearing in the corresponding definition included in formula (3.3) with their initial values $a_1(0)$ and $a_2(0)$ reported in Table 2. Thus, after the reduction of the constants of motion, the Hamiltonian describing the three-body planetary problem can be expressed as a function of four pairs of canonical variables: $\boldsymbol{L} = \boldsymbol{\Lambda} - \boldsymbol{\Lambda}^*$, λ, ξ and η. We can introduce the secular model at order two in the masses thanks to the following three operations: we perform a first step of normalization

https://doi.org/10.1017/S1743921322000461 Published online by Cambridge University Press

aiming to reduce the perturbing part that does not depend on $\boldsymbol{L}$ and does depend on the angles λ; we put $\boldsymbol{L} = \boldsymbol{0}$ (this is made because we expect that the oscillations of the semi-major axes close to their initial values have negligible effects); we finally average over the mean anomalies $\boldsymbol{\lambda}$ (as it is usual, when the analysis is focused on the long-term evolution of a planetary system). Therefore, we can write our secular Hamiltonian model as follows:

$$H^{(\mathrm{sec})}(\boldsymbol{\xi}, \boldsymbol{\eta}) = \sum_{s=1}^{N_S/2} h_{2s}^{(\mathrm{sec})}(\boldsymbol{\xi}, \boldsymbol{\eta}) \ , \tag{3.4}$$

where h_{2s} is an homogeneous polynomial of degree $2s$. This means that the expansion contains just terms of even degree, as a further consequence of the well known D'Alembert rules. Let us stress that the canonical variables $(\boldsymbol{\xi}, \boldsymbol{\eta})$ appearing in formula (3.4) are not the ones defined in (3.3), by abuse of notation. Indeed, the former variables are obtained from the latter ones, by performing the canonical transformation defined by the normalization step introducing the secular model at order two in the masses. Since this change of variables differs from the identity, because of a small correction that is of order one in the masses, then the values of the canonical variables $(\boldsymbol{\xi}, \boldsymbol{\eta})$ appearing in formula (3.4) are quite close to the corresponding ones that are defined in (3.3). These last comments joined with the remark that both ξ_j and η_j are $\mathcal{O}(e_j)$ for $e_j \to 0 \ \forall \, j = 1, 2$ (as it can be easily checked by looking at the definition (3.3)) allow us to give a meaning to the parameter N_S , in the sense that $H^{(\mathrm{sec})}$ provides an approximation of the secular dynamics up to order N_S in the eccentricities. On the one hand, in practical applications one is interested in expansions up to high order in eccentricities†; on the other hand, the computational effort critically increases with respect to N_S . To fix the ideas, in the case of the υ Andromedæ planetary system we have found that setting $N_S = 8$ is a good balance between these two different needs that are in opposition to each other.

We have explicitly performed all the computations of Poisson brackets (required by Lie series formalism to express canonical transformations) and all the expansions briefly described in the present section, by using *Χρόνος*. It is a software package especially designed for doing computer algebra manipulations into the framework of Hamiltonian perturbation theory (see Giorgilli & Sansottera 2012 for an introduction to its main concepts). Such computations also allow an easy visualisation of the secular dynamics by adopting a classical tool in the context of the numerical investigations: the Poincaré sections. In fact, we have performed many numerical integrations of the secular model $H^{(\mathrm{sec})}$ that is defined in (3.4) by simply applying the RK4 method‡.

A few dynamical features of the Hamiltonian model defined by $H^{(\mathrm{sec})}$ are summarised in the plots reported in Fig. 3. The orbit plotted in red in both panels refers to a set of initial conditions of the same type with respect to those considered in the previous Section 2. In detail, the initial values of the mean anomalies have been set so that $M_1(0) = M_2(0) = 0°$, while the other initial conditions are taken from the mid values of Table 1 (for what concerns $\iota(0)$, $\omega(0)$ and $\Omega(0)$ only) and from Table 2 (for the remaining data). Since the Poincaré sections are plotted in correspondence to the hyperplane $\eta_2 = 0$ (with the additional condition $\xi_2 > 0$) and the canonical variables $(\boldsymbol{\xi}, \boldsymbol{\eta})$ appearing in formula (3.4) are close to those defined in (3.3), then we can assume that on the surface of section $\omega_2 \simeq 0$. In the left panel of Fig. 3, therefore, the difference of the pericentre

† However, it must be taken into account that too large expansions of the secular model introduced here can be meaningless, because the high quality of the approximation in the eccentricities can be shadowed by the lack of precision with respect to the masses.

‡ It is very well known that long-term numerical integrations of secular models are much less computationally expensive than those dealing with the corresponding complete planetary system (see, e.g., Laskar 1988 and the references therein).

https://doi.org/10.1017/S1743921322000461 Published online by Cambridge University Press

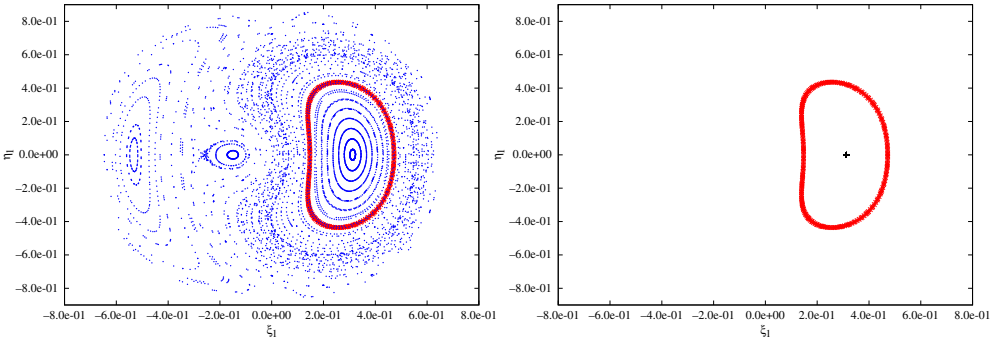

Figure 3. On the left, Poincaré sections that are corresponding to the hyperplane $\eta_2 = 0$ (with the additional condition $\xi_2 > 0$) and are generated by the flow of the Hamiltonian secular model $H^{(\mathrm{sec})}$, given in (3.4) at order two in the masses for the exoplanetary system υ Andromedæ; the orbit in red refers to the motion starting from initial conditions of the same type of those considered in Figs. 1–2 with the additional choice of the initial mean anomalies, that have been fixed so that $M_1(0) = M_2(0) = 0^\circ$. On the right panel, the same orbit in red is shown: approximately at its centre the symbol + represents the orbit of a one-dimensional elliptic torus (that reduces to a fixed point in these Poincaré sections). See the text for more details.

arguments $\omega_2 - \omega_1$ is evaluated by the polar angle, whose width is measured, as usual, with respect to the set of the positive abscissas, i.e., $\{(\xi_1 > 0, \eta_1 = 0)\}$. Thus, we can easily appreciate that this angle is librating around 0° also in the case of the secular model, in agreement with the corresponding plots reported in Figs. 1–2, that refer to the dynamics of the complete planetary system. By taking into account the fact that the nodes are opposite in the Laplace frame, this means that the pericentres of υ And c and υ And d are in the so-called apsidal locking regime in the vicinity of the anti-alignment of the pericentres. It is easy to remark that the Poincaré sections plotted in red (that are corresponding to the motion starting from the initial conditions we have chosen to consider) are orbiting around a fixed point, whose presence is also highlighted in the right panel of Fig. 3. Let us recall that all the Poincaré sections reported in Fig. 3 refer to the same level of energy, say E, corresponding to the set of the initial conditions we have previously described. Since $H^{(\mathrm{sec})}$ is a two degrees of freedom Hamiltonian, the manifold labelled by such a value of the energy will be three-dimensional; in other words, by plotting the Poincaré sections, we automatically reduce by one the dimensions of the orbits. This is the reason why a fixed point actually corresponds to a periodic orbit. Since such a fixed point with positive value of the abscissa is surrounded by closed curves, then we can argue that such a periodic orbit is linearly stable for what concerns the transverse dynamics. This means that it can be seen as a one-dimensional elliptic torus. Therefore, we can conclude that the orbit which intersects the hyperplane $\eta_2 = 0$ in correspondence with the red dots is actually winding around a linearly stable periodic orbit, by remaining in its vicinity. This explains why it can be convenient to adopt a strategy based on two different algorithms: the first one refers to the elliptic torus (that corresponds to a fixed point in the Poincaré sections) and provides a good enough approximation to start the second computational procedure that constructs the final KAM torus (which shall include also the points marked in red in Fig. 3).

3.2. *Construction of the normal form for an one-dimensional elliptic torus*

It is now convenient to introduce a new set of canonical coordinates by including among them also an angle which describes the libration of the difference of the pericentre arguments, i.e., $\omega_2 - \omega_1$. For such a purpose, we first introduce a set of action-angle

https://doi.org/10.1017/S1743921322000461 Published online by Cambridge University Press

variables $(\boldsymbol{\mathcal{J}}, \boldsymbol{\psi})$ via the canonical transformation

$$\xi_j = \sqrt{2\mathcal{J}_j}\cos\psi_j \ , \qquad \eta_j = \sqrt{2\mathcal{J}_j}\sin\psi_j \ , \qquad \forall\ j = 1, 2, \tag{3.5}$$

being $(\boldsymbol{\xi}, \boldsymbol{\eta})$ the variables appearing as arguments of the secular Hamiltonian $H^{(\mathrm{sec})}$ defined in (3.4). Then, we define a new set of variables $(\boldsymbol{I}, \boldsymbol{\vartheta})$ such that

$$\vartheta_1 = \psi_1 - \psi_2 \ , \quad \vartheta_2 = \psi_2 \ , \quad I_1 = \mathcal{J}_1 \ , \quad I_2 = \mathcal{J}_2 + \mathcal{J}_1 \ . \tag{3.6}$$

In view of the discussion included in the previous subsection, we have that the angle $\vartheta_1 \simeq \omega_2 - \omega_1$ is expected to librate in the model under consideration. We now move to (new) canonical polynomial variables $(\boldsymbol{x}, \boldsymbol{y})$ defined as

$$x_j = \sqrt{2I_j}\cos\vartheta_j \ , \qquad y_j = \sqrt{2I_j}\sin\vartheta_j \ , \qquad \forall\ j = 1, 2 \ . \tag{3.7}$$

Let us also remark that making Poincaré sections with respect to the hyperplane $\eta_2 = 0$, when $\xi_2 > 0$ is equivalent to impose $\psi_2 = 0$, because of the definitions in (3.5). Therefore, looking at formulæ (3.6)–(3.7), one can easily realise that the drawing in the left panel of Fig. 3 can be seen as a plot of the Poincaré sections in coordinates $(x_1\ ,\ y_1)$ with respect to $y_2 = 0$ and with the additional condition $x_2 > 0$. By a simple numerical method, we can easily determine the initial condition $(\boldsymbol{x}^\star, \boldsymbol{y}^\star)$ that is in correspondence with a Poincaré section and generates a periodic solution. We can now subdivide the variables in two different pairs. The first one is given by $(p, q) \in \mathbb{R} \times \mathbb{T}$, i.e., the action-angle pair describing the periodic motion. Thus, we rename the angle ϕ_2 as q, while the action is obtained by translating the origin of I_2 so that $p = I_2 - \left((x_2^\star)^2 + (y_2^\star)^2\right)/2$. For what concerns the second pair of canonical coordinates, we start from the polynomial variables (x_1, y_1) in order to describe the motion transverse to the periodic orbit. It is now convenient to rescale the transverse variables $(\bar{x}_1, y_1)$, being $\bar{x}_1 = x_1 - x_1^\star$, in such a way that the Hamiltonian part which is quadratic in the new variables (x, y) and does not depend on (p, q) is in the form $\Omega^{(0)}(x^2 + y^2)/2$. This rescaling can be done by a canonical transformation as the quadratic part does not have any mixed term $\bar{x}_1 y_1$ and the coefficients of $\bar{x}_1^2$ and y_1^2 have the same sign, because of the proximity to an elliptic equilibrium point. Thus, since such a quadratic part is in the preliminary form $a\bar{x}_1^2 + b y_1^2$, it suffices to define the new variables (x, y) as $x = \sqrt[4]{\frac{a}{b}}\,\bar{x}_1$, $y = \sqrt[4]{\frac{b}{a}}\,y_1$. Finally, we introduce the second pair of canonical coordinates $(J, \phi) \in \mathbb{R}_+ \cup \{0\} \times \mathbb{T}$ so that $x = \sqrt{2J}\cos\phi$ and $y = \sqrt{2J}\sin\phi$.

After having performed all the canonical transformation described above, the Hamiltonian can be written in the following way:

$$\mathcal{H}^{(0)}(p, q, J, \phi) = \mathcal{E}^{(0)} + \nu^{(0)} p + \Omega^{(0)} J + h(p, J, \phi) + \varepsilon f^{(0)}(p, q, J, \phi) \ , \tag{3.8}$$

where $\mathcal{E}^{(0)}$ is constant (that is close to the energy value of the wanted periodic orbit), $\nu^{(0)}$ and $\Omega^{(0)}$ are angular velocities, the function $h(p, J, \phi) = \mathcal{O}(\|(p, J)\|^{3/2})$ when the action vector† $(p, J) \to \mathbf{0}$ and $\varepsilon f^{(0)}(p, q, J, \phi)$ is a generic perturbing term, with ε playing the role of the small parameter. If such a perturbation is small enough, then it is possible to successfully perform a normalization algorithm, which allows to construct another canonical transformation Φ that conjugates the initial Hamiltonian $\mathcal{H}^{(0)}$ to $\mathcal{H}^{(\infty)} = \mathcal{H}^{(0)} \circ \Phi$ having the following (normal) form:

$$\mathcal{H}^{(\infty)}(P, Q, X, Y) = \mathcal{E}^{(\infty)} + \nu^{(\infty)} P + \frac{\Omega^{(\infty)}}{2}\left(X^2 + Y^2\right) + \mathcal{R}(P, Q, X, Y) \ , \tag{3.9}$$

where $\mathcal{E}^{(\infty)}$ is constant, $\nu^{(\infty)}$ and $\Omega^{(\infty)}$ are angular velocities and the remainder $\mathcal{R}$ is such that $\mathcal{R}(P, Q, X, Y) = o\big(|P| + \|(X, Y)\|^2\big)$, when $(P, X, Y) \to (0, 0, 0)$. Therefore, one

† Because of the change of coordinates which introduces the canonical pair of variables (J, ϕ), i.e., $x = \sqrt{2J}\cos\phi$ and $y = \sqrt{2J}\sin\phi$, also semi-integer powers of J can appear in the expansion (3.8) of the Hamiltonian $\mathcal{H}^{(0)}$.

https://doi.org/10.1017/S1743921322000461 Published online by Cambridge University Press

can easily check that

$$(P(t), Q(t), X(t), Y(t)) = \big(0, Q(0) + \nu^{(\infty)} t, 0, 0\big) \tag{3.10}$$

is a solution of the Hamilton equations, since the function $\mathcal{H}^{(\infty)}$, contains terms of type $\mathcal{O}(P^2)$, $\mathcal{O}(|P|\|(X,Y)\|)$ and $\mathcal{O}(\|(X,Y)\|^3)$ only, except for its main part (that is made by a constant, a linear term in P and another quadratic in both X and Y). Because of this remark, it is evident that the 1D manifold $\big\{(P,Q,X,Y) : P=0,\ Q\in\mathbb{T},\ X=Y=0\big\}$ is invariant. The energy level of such a solution is equal to $\mathcal{E}^{(\infty)}$. The elliptical character is given by the fact that, in the remaining degree of freedom, the transverse dynamics is given by an oscillatory motion whose period tend to the value $2\pi/\Omega^{(\infty)}$, in the limit of $(P,X,Y)\to(0,0,0)$. Of course, this is due to the occurrence of the term $\Omega^{(\infty)}(X^2+Y^2)/2$ which overwhelms the effect of the remainder $\mathcal{R}$ in the so-called limit of small oscillations.

In the case under study, dealing with the exoplanetary system υ Andromedæ, the normalization algorithm can be adapted so as to construct the 1D elliptic torus with a value of the parameter $\mathcal{E}^{(\infty)}$ equal to the energy level of the Poincaré sections (Caracciolo et al. 2022). In the right panel of Fig. 3 all the intersections of the corresponding orbit with the Poincaré surface $\eta_2=0$ are marked with a black cross. Of course, they perfectly superpose each other in a single fixed point corresponding to the wanted periodic orbit. In Caracciolo (2021), the normalization algorithm we have adopted to construct elliptic tori is fully described and its convergence is thoroughly analysed from a theoretical point of view. In short, such a procedure can be made in strict analogy with the construction of the Kolmogorov normal form. In fact, it can be formulated in such a way to introduce a sequence of Hamiltonians $H^{(r)}$ that are iteratively defined by a normalization step that is mainly composed by three Lie series: the first aims to reduce the perturbation that is not depending on the actions (p,J); the second achieves the same with the terms proportional to $\sqrt{J}$; also the third has the same goal for what concerns the terms that are linear in p or in J. We remark that in the normal form Hamiltonian $\mathcal{H}^{(\infty)}$ written in (3.9) we have expressed the dynamics that is transverse to the 1D elliptic torus in terms of the normalised canonical coordinates (X,Y) of polynomial type (instead of using action–angle variables), in order to highlight the existence of the periodic solution (3.10).

3.3. *Final construction of the invariant KAM torus*

It is now convenient to express also the second pair of canonical coordinates appearing in the normalised Hamiltonian (3.9) in the form of action–angle variables, i.e., we introduce (I,Θ) so that $X=\sqrt{2I}\cos\Theta$ and $Y=\sqrt{2I}\sin\Theta$. A very simple canonical change of variables, i.e.,

$$p_1 = P\,, \quad q_1 = Q\,, \quad p_2 = I - I^\star\,, \quad q_2 = Q\,, \tag{3.11}$$

is now enough in order to transform the Hamiltonian $\mathcal{H}^{(\infty)}$ (introduced at the end of the previous subsection) to $H^{(0)}(\boldsymbol{p},\boldsymbol{q}) = \boldsymbol{\nu}\cdot\boldsymbol{p} + h^{(0)}(\boldsymbol{p},\boldsymbol{q}) + \varepsilon f^{(0)}(\boldsymbol{p},\boldsymbol{q})$, that is in a suitable form to start the classical normalization algorithm that is the base of the proof scheme of KAM theorem. In a first approximation, the translation constant can be determined as $I^\star = (X_0^2+Y_0^2)/2$, where $(X_0\,,\,Y_0)$ are values of the canonical coordinates (X,Y) corresponding to the initial conditions. Moreover, as a preliminary step we determine the angular velocity vector $\boldsymbol{\nu}$ by using the frequency analysis method. The choice of $I^\star$ can be optimised by applying a Newton method, so as to approach as much as possible the vector $\boldsymbol{\nu}$ (Caracciolo et al. 2022). Fig. 4 highlights that the algorithm constructing the Kolmogorov normal form (3.2) is successful also for the initial conditions considered in the present section, i.e., with mean anomalies fixed so that $M_1(0)=M_2(0)=0^\circ$, while

https://doi.org/10.1017/S1743921322000461 Published online by Cambridge University Press

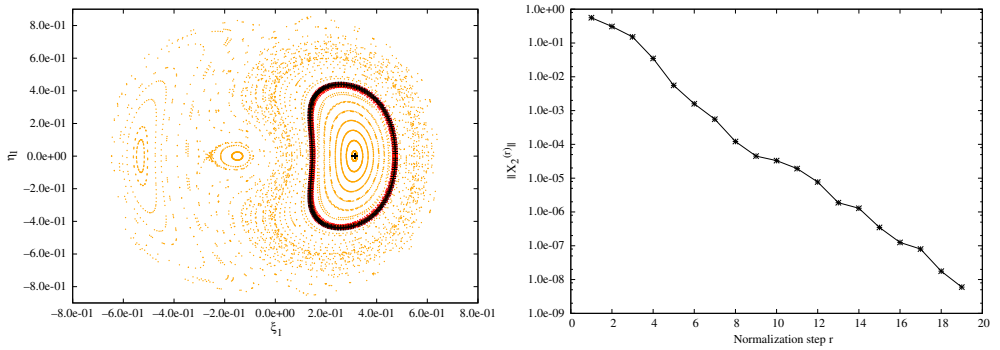

Figure 4. On the left, comparisons between the Poincaré sections generated by two different initial conditions. The first ones are marked in red and are exactly the same as those appearing in the left panel of Fig. 3 (where they are plotted in red as well). The second ones are marked in black and correspond to the orbit on the invariant KAM torus. The other "background" Poincaré sections are defined in the same way as those reported in Fig. 3; in particular, the dots plotted in blue there are located exactly in the same positions as those marked in orange here. The black symbol + refers to the orbit of the 1D elliptic torus also here. On the right, the behaviour of $\|\chi_2^{(r)}\|$ is plotted as a function of the normalization step r.

the other initial conditions are taken from the mid values of Table 1 (for what concerns $\iota(0)$, $\omega(0)$ and $\Omega(0)$ only) and from Table 2 (for the remaining data). In the left panel the Poincaré sections that are plotted (in red) during the numerical integration of the equations of motion related to the Hamiltonian (3.4) perfectly superpose to the orbit produced by composing all the canonical transformations briefly described in the present section, which is marked in black. The right panel of Fig. 4 clearly shows the regularity of the decrease of the norms of the generating functions (which are computed by simply adding up the absolute values of all the Taylor–Fourier coefficients). This gives a clear numerical indication of the convergence of the computational procedure in the case under study dealing with the exoplanetary system υ Andromedæ.

We stress that the importance of the translation constant $I^\star$ is crucial. Indeed, the abundance of the KAM manifolds surrounding an invariant torus is an increasing function of the inverse of the distance from said torus (as it has been shown, e.g., in Morbidelli & Giorgilli 1995). This is in agreement with the rather well known fact that the small parameter ε, which enters in the definition of the Hamiltonian $H^{(0)}$, is proportional to the shift value $I^\star$ (see, e.g., Giorgilli et al. 2017). Therefore, also the rate of the exponential decrease of the generating functions depends on $I^\star$: the smaller the latter the faster the former. In other words, we can also say that the invariant tori surrounding a reference one are more and more *robust* when the shift value $I^\star$ tends to zero. This means that larger and larger additional perturbing terms are needed in order to destroy this invariant structure for $I^\star \to 0$. Of course, all these remarks still hold true also when the reference torus (corresponding to $I^\star = 0$) is of elliptic type, as it is in the case of the periodic orbit $(P(t), Q(t), X(t), Y(t)) = \big(0, Q(0) + \nu^{(\infty)} t, 0, 0\big)$ that is obviously invariant with respect to the Hamiltonian flow of the normal form $\mathcal{H}^{(\infty)}$ written in (3.9).

4. The criterion of the minimal area as a robustness indicator

4.1. *Motivation and definition*

In the final discussion at the end of the previous section, we have explained why the shift value $I^\star$ appearing in the canonical transformation (3.11) can be considered

https://doi.org/10.1017/S1743921322000461 Published online by Cambridge University Press

as a good indicator of the dynamical robustness of an eventually existing KAM torus. However, such a concept is not easy to use in the context of numerical explorations, because its computation would require to preliminarily construct the normal forms we have previously described. Here, we are going to make the effort to reformulate our approach in a way that is far more handy in view of practical applications.

Firstly, let us remark that from the definition (3.11) it immediately follows that the shift value $I^\star$ has the physical dimensions of an action. Let us also recall that in Hamiltonian systems having one degree of freedom, the action is usually introduced as the area contoured by a closed orbit (see, e.g., § 50 of Arnold 1989). Since the action $I = (X^2 + Y^2)/2$ is a sort of squared distance in the pair of canonical coordinates (X, Y) which describe the transverse dynamics with respect to the 1D elliptic torus, then it looks rather natural to transfer the role of robustness indicator from the quantity $I^\star$ to the area enclosed by an orbit in the Poincaré sections. Let us directly refer to Fig. 3 in order to fix the ideas. We recall that we have adopted the non-normalised canonical coordinates $(\boldsymbol{\xi}, \boldsymbol{\eta})$ to plot those Poincaré sections, instead of (X, Y) that are much more expensive to compute. Nevertheless, in the hyperplane $\eta_2 = 0$ (after having fixed the energy level) the pair $(\xi_1\,,\,\eta_1)$ evidently describes a manifold that is transverse to the 1D elliptic torus, which is located by a fixed point marked with a black cross in the right panel. Since all the invariant tori winding around that periodic orbit describe Poincaré sections which are enclosing each other, then we can assume that the area embraced by the Poincaré sections is proportional to the distance (in action) from the elliptic torus. Therefore, by combining all the arguments explained at the end of the previous section with those discussed at the beginning of the present one, it is natural to assume that *an invariant torus is as more robust as smaller is the area contoured by the corresponding Poincaré sections*.

We now come to the approximated evaluation of such an area. By focusing our attention on the Poincaré sections marked in red in both panels of Fig. 3, we can say that the corresponding area is nearly equal to

$$\left(\max_t \left\{\xi_1(t)\right\} - \min_t \left\{\xi_1(t)\right\}\right) \left(\max_t \left\{\eta_1(t)\right\} - \min_t \left\{\eta_1(t)\right\}\right) \,. \tag{4.1}$$

Let us recall that ξ_1 and η_1 are proportional to $e_1 \cos\omega_1$ and $e_1 \sin\omega_1$, respectively, as determined by the definitions (3.3). Therefore, we can assume that also the area written in the formula above is proportional to

$$\mathcal{A} = \left[\left(e_{1;\max}\right)^2 - \left(e_{1;\min}\right)^2\right] \max_t \left|\omega_1(t) - \omega_2(t)\right| \,, \tag{4.2}$$

where the meaning of the new symbols we have just introduced is $e_{1;\max} = \max_t \left\{e_1(t)\right\}$ and $e_{1;\min} = \min_t \left\{e_1(t)\right\}$. Moreover, in order to write the definition of the quantity $\mathcal{A}$ above as an approximation of the action surface written in formula (4.1), we have also assumed that (by symmetry reasons) both the extremals $\max_t\{\xi_1(t)\}$ and $\min_t\{\xi_1(t)\}$ are in correspondence with $\omega_1 = 0$, while we have evaluated the width $\max_t\{\eta_1(t)\} - \min_t\{\eta_1(t)\}$ with a circular arc centred in the origin $(\xi_1\,,\,\eta_1) = \mathbf{0}$ of the frame of the Poincaré surface. We remark that the half-width of that arc is evaluated by referring to $\left|\omega_1(t) - \omega_2(t)\right|$, because ω_2 is equal to zero in the region of the Poincaré surface with $\xi_1 > 0$ and we want to evaluate the quantity $\mathcal{A}$ for any motion in librational regime with respect to the difference of the pericentre arguments.

We can summarise all the discussion above by formulating the following

robustness criterion: we assume that a **quasi-periodic Hamiltonian motion describing an invariant torus** *is as more robust as smaller is the corresponding quantity* $\mathcal{A}$ *defined in* (4.2).

https://doi.org/10.1017/S1743921322000461 Published online by Cambridge University Press

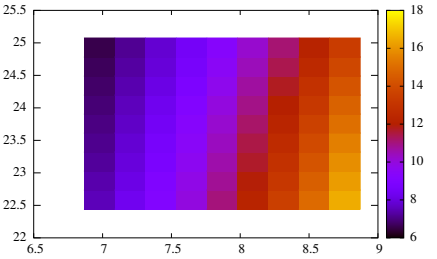

	υ And c	υ And d
m $[M_J]$	15.9792	9.9578
$a(0)$ [AU]	0.829	2.53
$e(0)$	0.239	0.31
$\iota(0)$ [°]	6.865	25.074
$M(0)$ [°]	355	335
$\omega(0)$ [°]	245.809	254.302
$\Omega(0)$ [°]	229.325	7.374

Figure 5. On the left, colour-code plot of the area $\mathcal{A}$ for different initial values of the inclinations $\iota_1(0)$ and $\iota_2(0)$. See formula (4.2) for the definition of the quantity $\mathcal{A}$. On the right, Table including the values of the masses and the initial conditions expected to correspond to the most robust planetary orbit compatible with the observed data available for υ And c and υ And d, according to the criterion of the minimal area.

It is quite evident that the statement above requires to minimise the area enclosed by the Poincaré sections, when we look for the most robust orbit originating from a set of possible initial conditions. For short, hereafter, we will refer to that as the criterion of the "minimal area".

4.2. *An application to the υ Andromedæ extrasolar planetary system*

In spite of the fact that we have constantly referred to a *secular* model in order to introduce and motivate our robustness criterion, we emphasise that its formulation is so flexible that it can be applied also to the study of the *complete* planetary dynamics of extrasolar systems. As we have claimed since the Introduction of the present work, we are going to select a set of initial conditions that is corresponding to an orbital configuration of the υ Andromedæ three-body model which is extremely stable. In our opinion, looking for *robust* invariant tori with a numerical criterion inspired by the secular dynamics has a twofold meaning. Firstly, they have more chances to persist when the perturbing effects due to the fast dynamics are taken into account; as we have shown in Section 2, chaotic motions compatible with the initial conditions are not rare in a probabilistic sense. Moreover, *robust* invariant tori describing the orbits υ And c and υ And d are expected to stay within a dynamically stable region of the phase space also when the effects due to υ And b and/or υ And e are included in the model.

In order to avoid the extensive study of a grid of initial conditions having a too high dimensionality, we will split our analysis in three different layers. As a first step, we consider initial conditions such that the mean anomalies are fixed so that $M_1(0) = M_2(0) = 0°$, while $\boldsymbol{\omega}(0)$ and $\boldsymbol{\Omega}(0)$ are taken from the corresponding mid values of Table 1; moreover, the assumed values of $\boldsymbol{a}(0)$, $\boldsymbol{e}(0)$ and minimal masses come from Table 2; the initial data are completed by covering the range of values of $\iota_1(0)$ and $\iota_2(0)$ which is reported in Table 1 with a regular grid of 10x10 points. For each of these 100 initial conditions, we numerically integrate the equations of motion, by using the symplectic method $\mathcal{SBAB}_{\mathcal{C}3}$ (also here we adopt the same integrator as in Section 2, which is described in Laskar & Robutel 2001, with the same total timespan and integration step, that are 10^5 yr and 0.02 yr, respectively), and we compute the corresponding value of the numerical indicator $\mathcal{A}$. The results are reported in the left panel of Fig. 5. A straightforward application of the minimal area criterion allows us to conclude that the initial conditions that are expected to correspond to the most robust planetary orbit are such that

$$\iota_1(0) = 6.865° \ , \quad \iota_2(0) = 25.074° \ , \quad \Longrightarrow \quad m_1 = 15.9792\, M_J \ , \quad m_2 = 9.9578\, M_J \ . \quad (4.3)$$

https://doi.org/10.1017/S1743921322000461 Published online by Cambridge University Press

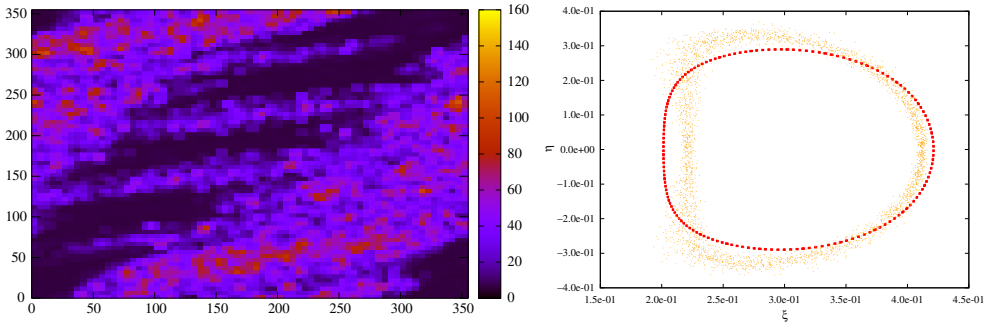

Figure 6. On the left, colour-code plot of the area $\mathcal{A}$ for different initial values of the mean anomalies $M_1(0)$ and $M_2(0)$. See formula (4.2) for the definition of the quantity $\mathcal{A}$. On the right, in orange, plot of the Poincaré sections that are corresponding to the hyperplane $\eta_2 = 0$ (with the additional condition $\xi_2 > 0$) and are generated by the flow of the complete Hamiltonian model of the exoplanetary system υ Andromedæ; such a motion is started from the initial conditions listed in the Table included on the right of Fig. 5. In red, plot of the Poincaré sections generated by the flow of the secular model $H^{(\mathrm{sec})}$, given in (3.4) and starting from initial conditions generated by those same values of the orbital elements.

The left panel of Fig. 5 clearly shows a rather surprising result: the most robust configurations correspond to the minimal value of the initial inclination $\iota_1(0)$ and, thus, to the maximal value of the υ And c mass (i.e., $\simeq 16\, M_J$). This conclusion is in agreement with a similar analysis that has been performed in Caracciolo et al. (2022), by studying the ratio between the norm of the last- and first-computed generating function, among those reported in a graph analogous to that appearing in the right panel of Fig. 4. The decrease rate of the sequence of the generating functions $\{\chi_2^{(r)}\}_{r\geq 1}$ (which are defined by the normalization algorithm eventually leading to the final Kolmogorov normal form) has been been firstly adopted as a robustness indicator starting from Volpi et al. (2018). We stress that this our new result looks to be rather unexpected when compared with the existing ones in the scientific literature: none of the four stable (and prograde) orbital configurations reported in Table 3 of Deitrick et al. (2015) is such that the υ And c mass is greater than $11\, M_J$, that is below the lowest possible value of $m_1 = 1.91/\sin(\iota_1(0))\, M_J$, where $1.91\, M_J$ is the minimal mass of υ And c taken from Table 2 and its initial inclination $\iota_1(0)$ is ranging in the corresponding interval reported in Table 1.

We continue our analysis by studying a second layer. We now consider initial conditions such that the mean anomalies are still fixed so that $M_1(0) = M_2(0) = 0°$, while $\boldsymbol{a}(0)$, $\boldsymbol{e}(0)$ are taken from Table 2 and the values of the initial inclinations and masses are as written in formula (4.3). In this second layer of analysis, the initial data are completed by covering the range of values of the angles $\boldsymbol{\omega}(0)$ and $\boldsymbol{\Omega}(0)$ with a regular 4D grid. Since the uncertainties on the knowledge of both the pericentre arguments and the longitudes of the node are not so large, we limit ourselves to define a grid which considers for each of the angles $\omega_1(0)$, $\omega_2(0)$, $\Omega_1(0)$, and $\Omega_2(0)$ just three possible values that are the minimum, the mid-point and the maximum of the corresponding values range reported in Table 1, respectively. For each of the so defined 81 initial conditions, we perform the same type of numerical integration we have described above. In this case, the application of the minimal area criterion leads to the conclusion that the initial values of $\boldsymbol{\omega}$ and $\boldsymbol{\Omega}$ that are expected to correspond to the most robust orbit are those reported in the Table included on the right of Fig. 5.

We come now to the description of the third layer of our analysis. In this last case, we consider the values of the planetary masses m_1 , m_2 and the initial conditions for the orbital elements $\boldsymbol{a}$, $\boldsymbol{e}$, $\boldsymbol{\iota}$, $\boldsymbol{\omega}$ and $\boldsymbol{\Omega}$ as they are given in the Table included on the right of

https://doi.org/10.1017/S1743921322000461 Published online by Cambridge University Press

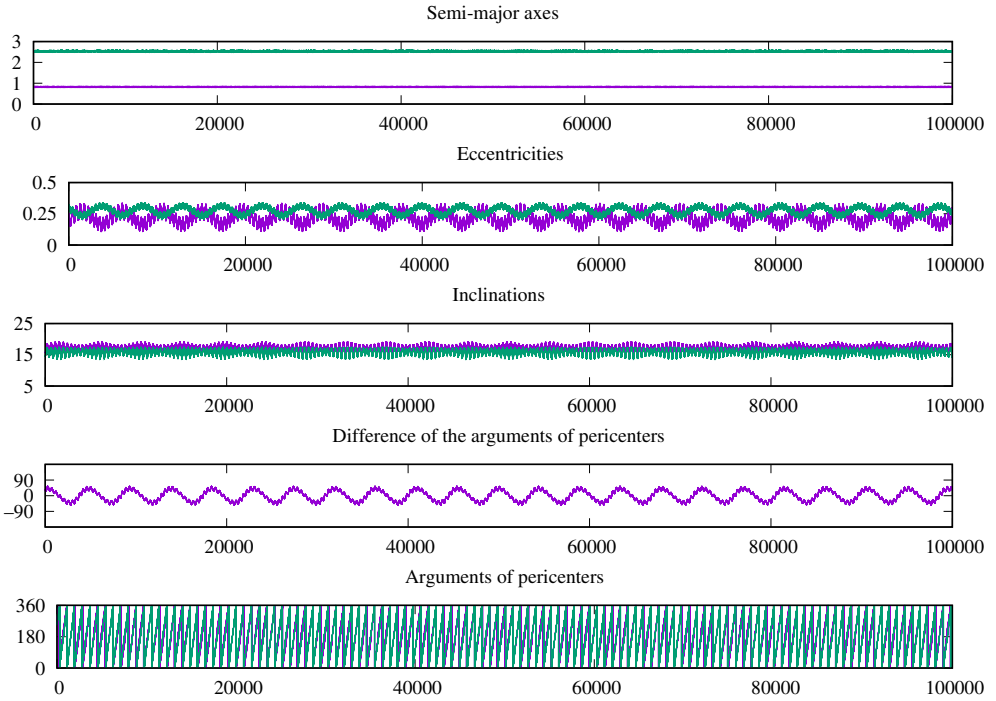

Figure 7. Orbital evolution of the exoplanets υ And c and υ And d in the case of the single set of initial conditions which is described in the Table included on the right of Fig. 5.

Fig. 5, while we make the coverage of all the possible initial values of the mean anomalies $\big\{\big(M_1(0), M_2(0)\big)\big\} \in [0°, 360°] \times [0°, 360°]$ by means of a regular 2D grid with a grid-step of 5°. Once again, for each of these $72^2 = 5184$ different initial conditions, we perform the same type of numerical integration we have described above. For all of them, we compute the quantity $\mathcal{A}$, that is defined in (4.2). The results are reported in the left panel of Fig. 6. By comparing that colour-code plot with those included in Fig. 1, we can appreciate that there is good agreement between them: the most robust regions (according to the criterion of the minimal area) look also well apart from possible collisions (because the eccentricity of the outer planet does not reach large values) and fairly inside the librational regime with respect to the difference of the pericentre arguments. The initial values of the mean anomalies that are expected to correspond to the most robust orbit are the following ones:

$$M_1(0) = 355° \ , \qquad M_2(0) = 335° \ . \tag{4.4}$$

In the right panel of Fig. 6, we have plotted the intersections of the corresponding "most robust" orbit with respect to the Poincaré hypersurface $\eta_2 = 0$. Moreover, we have done the same also for the flow of the Hamiltonian $H^{(\mathrm{sec})}$, which is defined in (3.4), starting from the corresponding initial conditions $\big(\boldsymbol{\xi}(0), \boldsymbol{\eta}(0)\big)$ that are computed in terms of the secular canonical coordinates. The comparison of these two different kinds of Poincaré sections allows us to conclude that, for what concerns the most robust orbit, the behaviour of the eccentricities in the case of the complete planetary Hamiltonian should be rather close to that we can observe in the secular model at order two in the masses.

Fig. 7 describes the dynamical evolution of the exoplanets υ And c and υ And d in the case of the orbit that we consider as the most robust, according to the analysis we have widely discussed in the present section. The comparison with the corresponding graphs

https://doi.org/10.1017/S1743921322000461 Published online by Cambridge University Press

that are reported in Fig. 2 allows us to appreciate that the behaviour has now become pleasantly quasi-periodic. Of course, this difference is entirely due to our accurate choice of the initial conditions.

5. Conclusions and perspectives

At the very beginning, our main motivation to start the investigations we have described in the present paper was essentially of mathematical character. Indeed, our aim was to select a set of initial conditions corresponding to an invariant KAM torus whose existence could have been proved rigorously. For such a purpose, the adoption of an approach based on a Computer-Assisted Proof (hereafter, CAP) is somehow unavoidable. In the last few years, the performances of CAPs have been improved so much that they are able to prove the existence of invariant tori for values of a small parameter (say, ε) that are amazingly close to the so called breakdown threshold, i.e., the critical value of ε beyond which the KAM manifold under study disappears (Figueras et al. 2017). For the time being, so-successful results have been obtained for benchmark systems (mappings with or without additional dissipative terms) that are quite interesting but intrinsically simple. On the other hand, the application of CAPs to realistic models of physical interest highlights that there is still a gap to fill in order to approach the numerical threshold (see, e.g., Calleja et al. 2022 and Valvo & Locatelli 2022; see also Caracciolo & Locatelli 2020 for the rigorous evaluation of an effective stability time, with a similar kind of CAP technique). This is the reason for which we were looking for initial conditions that were not only corresponding to an invariant torus (that could have been found by applying, e.g., the frequency analysis; see Laskar 2003), but also quite far from its breakdown threshold (which is somehow depending on the physical parameters characterising a planetary systems). This has been made with the hope that a rigorous proof of the existence of such a KAM manifold would have been so relatively easy to be completed even if the CAP technique we adopted needs further improvements, to be extensively applied to Hamiltonian models of physical interest. This strategy of ours has been successful: as it is discussed in Caracciolo et al. (2022), in the case of the secular dynamics of the υ Andromedæ planetary system we have been able to rigorously prove the existence of a KAM torus that is travelled by the motion law starting from the initial conditions we have selected and reported in the Table included on the right of Fig. 5.

In order to solve such a challenging problem, we have introduced a robustness criterion that we have named "of the minimal area". The practical implementation of this method of investigation is computationally inexpensive, making it suitable for extensive studies of extrasolar systems. Indeed, it just requires a few additional computations during the numerical integrations of the Hamilton equations, each of them starting from different initial conditions, that all together should give a reasonable coverage of a data range which is compatible with the observations. Our robustness criterion is also flexible enough to be applied jointly with numerical integrations of a complete planetary model or a secular one without any need of additional efforts for the adaptation. Moreover, the comparisons reported in the right panel of Fig. 6 shows that in the case of the selected initial conditions there is a good agreement between the Poincaré sections for the secular model at order two in the masses and those related to the complete planetary system. Since the fraction of the chaotic motions is expected to be much more relevant in the latter case than in the former one (according to the discussions and figures widely commented in Sections 2–3), this result is not a priori obvious and enforces our confidence in the accuracy of the secular model, at least in the region where the invariant tori are more robust.

In our opinion, the possible applications of our approach are not limited to problems which are interesting for reasons that are mainly mathematical. From an astronomical point of view, we think that the most interesting result described in this work of ours

https://doi.org/10.1017/S1743921322000461 Published online by Cambridge University Press

concerns with the masses of the planets in the υ Andromedæ system. Our analysis allow to conclude that configurations with a large mass of υ And c have to be considered as more probable, because they are more robust In other words, one can expect that configurations with larger values of the mass of υ And c are within a region that is extremely stable because it is filled by tori so robust that they can eventually persist also when other perturbing terms are considered. For instance, additional gravitational effects could be taken into account, because of the eventual reintroduction of υ And b and υ And e in the planetary model.

The conclusion we have commented just above could be thought as counter-intuitive, because one might expect that stability is always gained by decreasing the values of the planetary masses. On the other hand, the following easy remark could explain such a situation which appears in contradiction: for fixed values of the semi-major axes and the eccentricities, in the case of υ Andromedæ system, the configuration that we identify as the most robust among the possible ones is that reducing as much as possible the imbalance between the angular momenta† of υ And c and υ And d. It is natural to argue about the real meaning of such a possible explanation: is this just by chance or is it quite general that planetary stability is gained by a better balance of the angular momenta? If the latter statement holds true, under which conditions? We think that there are also other natural questions about the generality of our approach, which are mainly due to the fact that our robustness criterion has been devised by studying the secular dynamics of a planetary three-body problem in an apsidal locking regime. Could it be extended to systems where the difference of the arguments of the pericentres is in rotation? Could our approach be significantly adapted to systems hosting more than two exoplanets? In our opinion, all these questions deserve to be further investigated.

Acknowledgements

This work was partially supported by the MIUR-PRIN project 20178CJA2B – 'New Frontiers of Celestial Mechanics: theory and Applications'. The authors acknowledge also INdAM-GNFM and the MIUR Excellence Department Project awarded to the Department of Mathematics of the University of Rome 'Tor Vergata' (CUP E83C18000100006).

References

Arnold, V.I., 1963, *Russ. Math. Surv.*, 18, 9
Arnold, V.I., 1989, *Mathematical methods of classical mechanics*, 2nd edition, Springer-Verlag
Butler, R.P., et al., 1999, *Astroph. Jour.*, 526, 916
Calleja, R.C., Celletti, A., Gimeno, J., & de la Llave, R., 2022, *Commun. Nonlinear Sc. Numer. Simulat.*, 106, 106099
Caracciolo, C., 2021, *Math. in Engineering*, 4, 1
Caracciolo, C., & Locatelli, U., 2020, *Jour. of Comput. Dynamics*, 7, 425
Caracciolo, C., & Locatelli, U., 2021, *Commun. Nonlinear Sc. Numer. Simulat.*, 97, 105759
Caracciolo, C., Locatelli, U., Sansottera, M., & Volpi, M., 2022, *Mon. Not. Royal Astron. Soc.*, 510, 2147
Chiang, E.I., Tabachnik, S., & Tremaine, S., 2001, *Astron. Jour.*, 122, 1607

† The angular momenta of υ And c and υ And d are such that $\mathcal{G}_j = \Lambda_j(1 - \sqrt{1-e_j^2})$, with $\Lambda_j = m_0 m_j \sqrt{G(m_0+m_j)a_j}/(m_0+m_j)\ \forall\, j = 1, 2$. Looking at the data about semi-major axes, eccentricities and minimal masses that are reported in Table 2, one can easily check that the minimum difference between the angular momenta (i.e., $\mathcal{G}_2 - \mathcal{G}_1$) corresponds to the maximum possible value of the mass of the inner planet and the minimum of that of the outer one, which are $m_1 = 1.91/\sin(\iota_1(0))$ and $m_2 = 4.22/\sin(\iota_2(0))$, respectively, where the ranges of values of the initial inclinations $\iota_1(0)$ and $\iota_2(0)$ are reported in Table 1.

https://doi.org/10.1017/S1743921322000461 Published online by Cambridge University Press

Cloutier, R., et al., 2019, *Astron. & Astroph.*, 629, A111
Deitrick, R., et al., 2015, *Astroph. Jour.*, 798, 46
Figueras, J.-Ll., Haro, A., & Luque, A., 2017, *Found. Comput. Math.*, 17, 1123
Giorgilli, A., Locatelli, U., & Sansottera, M., 2009, *Cel. Mech. & Dyn. Astr.*, 104, 159
Giorgilli, A., Locatelli, U., & Sansottera, M., 2017, *Reg. & Chaot. Dyn.*, 22, 54
Giorgilli, A., & Sansottera, M., 2012, in P.M. Cincotta, C.M. Giordano & C. Efthymiopoulos (eds.), *Chaos, Diffusion and Non-integrability in Hamiltonian Systems*, Universidad Nacional de La Plata and Asociación Argentina de Astronomía Publishers
Kolmogorov, A.N., 1954, Engl. transl. in *Lecture Notes in Physics*, 1979, 93, 51
Laskar, J., *Astron. & Astroph.*, 1988, 198, 341
Laskar, J., 1989, *Notes scientifiques et techniques du Bureau des Longitudes* S026, available at https://www.imcce.fr/content/medias/publications/publications-recherche/nst/docs/S026.pdf
Laskar, J., 2003, in D. Benest, C. Froeschlé, & E. Lega E. (eds.), *Hamiltonian systems and Fourier analysis*, Taylor and Francis
Laskar, J., & Petit, A.C., 2017, *Astron. & Astroph.*, 605, A72
Laskar, J., & Robutel, P., 2001, *Cel. Mech. & Dyn. Astr.*, 80, 39
Libert, A.-S., Sansottera, M. 2013, *Cel. Mech. & Dyn. Astr.*, 117, 149
Locatelli, U., Caracciolo, C., Sansottera, M., & Volpi, M., 2022, in: G. Baù, S. Di Ruzza, R.I. Páez, T. Penati & M. Sansottera (eds.), *I-CELMECH Training School – New frontiers of Celestial Mechanics: theory and applications*, Springer PROMS (in press)
Locatelli, U., & Giorgilli, A., 2000, *Cel. Mech. & Dyn. Astr.*, 78, 47
Mayor, M., & Queloz, D., 1995, *Nature*, 378, 355
McArthur, B.E., et al., 2010, *Astroph. J.*, 715, 1203
McArthur, B.E., et al., 2014, *Astroph. J.*, 795, 41
Michtchenko, T.A., & Malhotra, R., 2004, *Icarus*, 168, 237
Morbidelli, A., & Giorgilli, A., 1995, *J. Stat. Phys.*, 78, 1607
Moser, J., 1962, *Nachr. Akad. Wiss. Gött., Math. Phys.*, 1, 1
Perryman, M., 2018, *The Exoplanet Handbook*, Cambridge Univ. Press, ISBN 9781108419772
Petit, A.C., Laskar, J., & Boué, G., 2017, *Astron. & Astroph.*, 607, A35
Sansottera, M., & Libert, A.-S., 2019, *Cel. Mech. & Dyn. Astr.*, 131, 38
Valvo, L., & Locatelli, U., 2022, *Jour. of Comput. Dynamics*, in press
Volpi, M., Locatelli, U., & Sansottera, M., 2018, *Cel. Mech. & Dyn. Astr.*, 130, 36